CMS PAS HIN-14-009

DRAFT
CMS Physics Analysis Summary

2015/05/27
Head Id: 284202
Archive Id: 90489:290297MP
Archive Date: 2015/04/11
Archive Tag: trunk

Measurement of prompt and non-prompt J/ψ production in pPb collisions at $\sqrt{s_{NN}} = 5.02$ TeV

The CMS Collaboration

Abstract

This document describes a J/ψ measurement in proton-lead collisions at a center-of-mass energy per nucleon pair of 5.02 TeV with an integrated luminosity of 34.6 nb^{-1} recorded by the CMS experiment at the LHC in 2013. Prompt J/ψ and non-prompt J/ψ from B hadron decays are separately measured via their $\mu^+\mu^-$ decay mode. The differential production cross section is presented with the center-of-mass rapidity of $-2.4 < y_{CM} < 1.93$ and the transverse momentum of $p_T < 30$ GeV/c. The ratio of the forward and backward production yields is measured in bins of p_T, rapidity, and the multiplicity-related variables. The prompt and non-prompt J/ψ yields at forward rapidities are relatively suppressed compared to backward rapidities. The tendency is more strongly marked for higher multiplicity event bins. Such an observation confirms the presence of cold nuclear matter effects in the J/ψ production in p-Pb.

This box is only visible in draft mode. Please make sure the values below make sense.

PDFAuthor:	Lamia Benhabib, Mihee Jo, Hyunchul Kim, Yongsun Kim, Kisoo Lee, Songkyo Lee
PDFTitle:	Jpsi production in pPb collisions
PDFSubject:	CMS
PDFKeywords:	physics, dimuons, proton Lead, charmonia, suppression, quark gluon plasma, shadowing

Please also verify that the abstract does not use any user defined symbols

1 Introduction

Understanding the production mechanisms of $c\bar{c}$ bound states, from first principle calculations based on quantum chromodynamics (QCD), remains an open question in proton-proton (pp) and heavy-ion collisions [1–8]. In pp collisions, despite the extensive progress [9–11], none of the existing models can reproduce simultaneously the cross sections and polarization results measured experimentally [12]. While the non-relativistic (NRQCD) approach can accurately describe the differential cross sections, it fails reproducing the polarization of prompt J/ψ measurements at LHC energies [13–18]. In relativistic heavy ion experiments carried out at SPS [6, 19, 20], RHIC [21, 22] and LHC [7, 23], a suppression of J/ψ and $\psi(2S)$ yields over a wide rapidity and p_{T} range has been observed for increasingly central collisions. Those results are consistent with expectations for the formation of a Quark Gluon Plasma (QGP) phase at temperatures where the $c\bar{c}$ bound state dissociates due to the screening of the color potential by surrounding quarks and gluons. [2, 24–26].

Apart from effects due to the hot and dense QGP medium, several other processes can affect the quarkonia production yields. Initial-state modifications of the parton distribution function (PDF) of a nucleus compared to that from protons, in particular, in the shadowing regime at low Bjorken-x (x), the quarkonia yields can be reduced since gluon-gluon collisions are their dominant production mechanism. Also, some theoretical models attribute the quarkonia suppression to the modification of $c\bar{c}$ pair's invariant mass [27, 28] or to the gluon radiation induced by multiple scattering with the surrounding medium [29–31]. In this context, the study of charmonia in proton-nucleus collisions is a basic prerequisite in order to understand the "cold nuclear matter" effects that can modify their production yields without the necessary formation of a QGP.

This paper reports the analysis of J/ψ production in proton-lead collisions at $\sqrt{s_{\mathrm{NN}}} = 5.02\,\mathrm{TeV}$ collected with the Compact Muon Solenoid (CMS) detector in 2013. J/ψ's are reconstructed via their dimuon decay channel, in the muon tracking system that covers a wide kinematic range of $-2.4 < y_{CM} < 1.93$ and $p_{\mathrm{T}} < 30$ GeV/c. This corresponds to $2 \cdot 10^{-4} < x < 10^{-3}$ for the forward region and $10^{-2} < x < 4 \cdot 10^{-2}$ for the backward one, in case of $2 \to 1$ processes [32]. Prompt J/ψ and non-prompt J/ψ from B-meson decays are separated by means of secondary $\mu^+\mu^-$ vertices. The differential cross sections are measured as a function of p_{T} and rapidity. The ratio of the yields in the forward and backward rapidities is used to probe rapidity-dependent cold nuclear matter effects. In addition, the dependence of the forward-to-backward ratio as a function of event activity is studied.

2 CMS Detector

A detailed description of the CMS detector can be found in Ref [33]. Its central feature is a superconducting solenoid with an internal diameter of 6 m, providing a magnetic field of 3.8 T. Within the field volume are the silicon pixel and strip tracker , the crystal electromagnetic calorimeter, and the brass/scintillator hadronic calorimeter. The silicon pixel and strip tracker measures charged-particle trajectories in the range $|\eta| < 2.5$. It consists of 66 M pixel and 10 M strip sensor elements. Muons are detected in the range $|\eta| < 2.4$, with detection planes based on three technologies: drift tubes, cathode strip chambers, and resistive plate chambers. Because of the strong magnetic field and the fine granularity of the tracker, the muon p_{T} measurement based on information from the tracker alone has a resolution between 1 and 2% for typical muons in this analysis.

The CMS apparatus also has extensive forward calorimetry, including two steel/quartz-fiber

Čerenkov hadron forward calorimeters (HF), which cover $2.9 < |\eta| < 5.2$. These detectors are used for online event selection and impact parameter-like characterization of the events in pPb collisions, where impact parameter refers here to the distance between the two centers of incoming projectiles.

3 Definitions and Event Selection

The pPb dataset used in this analysis corresponds to an integrated luminosity of 34.6 nb^{-1}. The beam energies were 4 TeV for protons, and 1.58 TeV per nucleon for the lead nuclei, resulting in a center-of-mass energy per nucleon-nucleon pair $\sqrt{s_{\mathrm{NN}}}$ of 5.02 TeV. The direction of the higher-energy proton beam was initially set up to be clockwise, and was reversed after 20 nb^{-1} to study systematic effects. As a result of the beam energy difference, the nucleon-nucleon center-of-mass in pPb collisions is not at rest with respect to the laboratory frame. Massless particles emitted at $|\eta_{CM}| = 0$ in the nucleon-nucleon center-of-mass frame are detected at $\eta_{lab} = -0.465$ for the first run period(clockwise proton beam) and $+0.465$ for the second run period (counterclockwise proton beam) in the laboratory frame. In the center-of-mass frame, forward regions (positive pseudorapidity) are defined by the proton-going direction. Data from two different directions are fitted separately for the signal extraction and then merged after the acceptance and efficiency corrections. The result presented here are based on dimuon events selected by the Level-1 (L1) trigger, an online hardware-based trigger system requiring two muon candidates in the muon detectors with no explicit limitations in momentum or rapidity.

The collision selection criteria developed in [34] are applied to remove beam-gas and multiple collision events (pile-up). The longitudinal and transverse distance between the primary vertex having the highest number of associated tracks and the secondary vertex is used for removing pileup events to avoid the bias in characterizing the event activity variables.

4 Signal Extraction

The signal extraction procedure is similar to those used in previous CMS analyses of pp [14] and PbPb [7] collisions. The dimuon invariant-mass spectrum is fitted with an exponential function representing the underlying background and the sum of a Crystal Ball [35] and a Gaussian function representing signal peak. The signal functions have independent widths σ_{Gaus} and σ_{CB} to accommodate dimuon invariant-mass resolution, but share the common mean.

To separate the J/ψ from B decay, a "prompt-signal region" is defined using the pseudo-proper decay length, $\ell_{\mathrm{J}/\psi} = L_{xy}\, m_{\mathrm{J}/\psi} / p_{\mathrm{T}}$, where L_{xy} is the transverse decay length in the laboratory frame [36, 37]. The resolution model of the pseudo-proper decay length exploits the per-event error information provided by the covariance matrices of the primary and secondary vertex fits. The prompt J/ψ component is described by the resolution function, the sum of two Gaussians. One of them with the narrower width describes most of the parts. The other one with wider width, with a very small fraction, parameterizes the tail components from imperfect primary vertex alignments. The non-prompt component is modelled by an exponential decay function convolved with the resolution function, and the continuum background component by the sum of three exponential functions, a single-sided left, a single-sided right and a double-sided, also convolved with the resolution function.

The invariant-mass spectrum and the $\ell_{\mathrm{J}/\psi}$ distribution of $\mu^+\mu^-$ pairs are fitted simultaneously in an extended unbinned maximum likelihood fit, in bins of p_{T}, rapidity and the multiplicity-related variables, where the fraction of non-prompt to prompt J/ψ is a free parameter. Before the fitting procedure, the wider width of the resolution function is fixed by the prompt Monte-Carlo samples to retain the minimum of freedom and more stable fit results. The parameters describing the lifetime distributions of the background are determined by the fits to the side-bands of the invariant mass distribution, $2.6 < m_{\mu\mu} < 2.9$ GeV/c^2 and $3.3 < m_{\mu\mu} < 3.5$ GeV/c^2.

Figure 1 shows exemples of fit projections onto the mass (left) and $\ell_{J/\psi}$ axes (right), for muon pairs with $5 < p_{\mathrm{T}} < 6.5$ GeV/c in $-2.4 < y_{lab} < -1.97$ and with $14 < p_{\mathrm{T}} < 30$ GeV/c in $-0.47 < y_{lab} < 0.43$ from the 1st run subset.

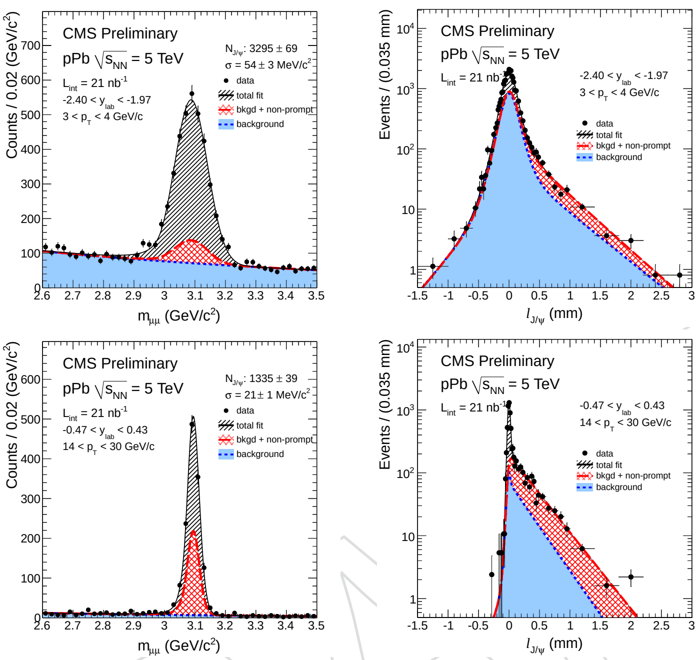

Figure 1: Invariant-mass (left) and pseudo-proper decay length distributions (right) of $\mu^+\mu^-$ pairs. The top panel represents the p_{T} range of $5 < p_{\mathrm{T}} < 6.5$ GeV/c in $-2.4 < y_{lab} < -1.97$, and the bottom panel represents the high p_{T} range of $14 < p_{\mathrm{T}} < 30$ GeV/c in $-0.47 < y_{lab} < 0.43$ from the 1st run subset. The projections of the two-dimensional fit function onto the respective axes are overlaid as black solid lines. The red dashed lines show the fitted contribution of non-prompt J/ψ. The fitted background contributions are shown by blue dotted lines.

5 Acceptance and efficiencies

Monte Carlo (MC) events are used to obtain acceptance and efficiency correction factors. J/ψ events are generated at 5.02 TeV using PYTHIA version 6.424 [38] and boosted in rapidity by -0.465 to account for the asymmetry of the beam energies. Samples for prompt and non-prompt J/ψ are independently produced using the D6T and Z2 tunes respectively. The prompt J/ψ samples are generated assuming no decay polarization, and the non-prompt J/ψ sample includes the polarization determined by the sum of the exclusive B hadron decays (B^+, B^-, B_s^0 and λ_b) from EVTGEN [39]. The final-state QED radiation of the decay muons is implemented using PHOTOS [40]. Finally, the CMS detector response is simulated using GEANT4 [41].

5.1 Acceptance

The dimuon signal's acceptance, A, is defined as the ratio of detectable dimuon pairs in the CMS detector within a restricted mass interval M to all generated pairs in a given (p_{T}, y) bin.

$$A(p_T, y) \quad = \quad \frac{N^{\mu^+\mu^-}_{detectable,M}(p_T, y)}{N_{generated}(p_T, y)} \tag{1}$$

where the numerator and denominator are defined in the following:

- $N^{\mu^+\mu^-}_{detectable,M}$: Number of dimuon signals in the MC simulation. Signals are declared to be detectable according to the cuts defined in the previous quarkonia analysis [14]. The mass interval M is [2.6, 3.5] GeV/c^2 in a given (p_T, y) bin.
- $N_{generated}$: Number of generated within geometrical coverage of the CMS muon detectors.

5.2 Efficiency correction

The dimuon reconsctruction efficiencies are acquired from MC simulation with furhter correction by a data-driven technique called *tag-and-probe* (T&P) in a similar way as in Ref. [7]. The data-to-MC ratios of single muon efficiencies, as a function of pseudo-rapidity and p_T, are calculated by T&P method. These ratios are applied as scale factors to convolve the dimuon efficiencies obtained in MC simulation, as accounted in Eq. 2.

$$\varepsilon = \varepsilon_{MC} \otimes \frac{\text{T\&P efficiency of } (\mu^+\mu^-)}{\text{MC efficiency of } (\mu^+\mu-)} \tag{2}$$

,where

$$\varepsilon_{MC} = \frac{\text{Number of reconstrcuted dimuon pairs}(p_T, y)}{\text{Number of generated dimuon pairs}(p_T, y)} \tag{3}$$

is the J/ψ efficiency without T&P correction. Only the dimuon pairs satisfying the acceptance criteria are considered in MC efficiency calculation. The amount of T&P correction is less than 5% for p_T above 5 GeV/c, and the largest correction is in 15% level for the lowest bins at the most forward and backward rapidities.

6 Systematic Uncertainties

The following sources of systematic uncertainties are considered in this measurement: signal extraction, acceptance and efficiency correction procedures. To estimate the systematic uncertainty due to the fitting procedure, the variation on the parameters or alternative fit functions have been considered for the mass and lifetime distributions. The differences compared to the nominal method are taken as systematic uncertainties. The detailed sources of the systematic uncertainty include the following:

- Variation of the signal lineshape in the dimuon mass distribution: In our default fit, we set the parameters of the CB tail $n_{CB} = 2.1$ and left α_{CB} as a free parameter. As alternative scenarios, we have either decreased or increased n_{CB} by 0.5. For α_{CB}, we fixed its values to $1, 2, 3$.
- Variation of the background fit function in the dimuon mass distribution: the straight line is tested and compare to the nominal single exponential function.
- Resolution model for the lifetime of prompt J/ψ: As a default, the width of wider Gaussian, σ_{wide} is fixed to prompt MC templates and the narrower width σ_{narrow} is

left free. For alternative options, we set both σ_{wide} and σ_{narrow} as free parameters. Secondly, both parameters are fixed to the MC templates.

- B lifetime model: alternative B lifetime model, based on MC templates [7] is tested and the difference in the fitted non-prompt fraction is taken as the systematic uncertainty.

The uncertainties tend to be larger for lower p_{T} and higher rapidity region and reach up to 24.2% for the prompt J/ψ component and 28.3% for the non-prompt. The data to MC discrepancy of the internal spectra in each p_{T} bin is the dominant source of systematic uncertainty in the acceptance and efficiency correction where the correction factors steeply changes. In order to correct this, the p_{T} distributions of MC samples are reweighted by the data/MC ratios for each rapidity bins to adjust the correction factors suitalbe for data spectra. The internal spectra ratio curve was interpolated by fitting data to MC ratio data points. The acceptance and efficiency uncertainties are estimated by comparing the values after p_{T} weighting with those before weighting, MC_{truth}.

In addition, the uncertainties of T&P corrections propagated to the uncertainties in efficiency are accounted by varying the fitting functions in the invariant mass distribution and by selecting higher quality T&P pairs to suppress the background level. The uncertainty due to acceptance correction is within 0.0 to 1.1% and those due the efficiency correction are within 2.1 to 23.5%, and tend to be larger for lower p_{T} bins.

Table 1 summaries different sources of systematic uncertainties described above in addition to the luminosity and the J/$\psi \to \mu^+\mu^-$ branching ratio. The largest uncertainty comes from the efficiency correction procedure.

Table 1: Summary of the relative systematic uncertainties on prompt and non-prompt J/ψ.

	prompt J/ψ (%)	non-prompt J/ψ (%)
Luminosity	3.5	3.5
Branching ratio	1	1
Yield extraction	1.0-6.3	1.6-15.8
Acceptance	0.0-1.1	0.0-0.8
Efficiency	2.1-21.6	2.1-23.5

7 Results

7.1 Production cross section

The production cross sections of prompt and non-prompt J/ψ are computed by

$$\frac{d^2\sigma}{dp_{\mathrm{T}}dy} = \frac{N_{fit}^{\mathrm{J}/\psi} / (A \cdot \varepsilon)}{L_{int} \times B(\mathrm{J}/\psi \to \mu^+\mu^-) \times \Delta p_{\mathrm{T}} \Delta y}, \quad (4)$$

where the variables are defined as follows:

- $N_{fit}^{\mathrm{J}/\psi}$ is the raw yield of J/ψ extracted from the fit procedure in a given (p_{T}, y) bin,
- A is the dimuon acceptance,
- ε is the dimuon efficiency,

- $L_{int} = (34.6 \pm 1.2)\ \mathrm{nb}^{-1}$ is the integrated luminosity,
- $B(\mathrm{J}/\psi \rightarrow \mu^+\mu^-) = (5.93 \pm 0.06)\%$ is the branching ratio to the $\mu^+\mu^-$ channel [42],
- Δp_T and Δy are the widths of the (p_T, y) bin.

In Figs 2 and 3, the double differential cross sections are plotted as a function of p_T in eight different rapidity ranges for prompt and non-prompt J/ψ respectively. The bin abscissae are given by the bin-averaged values. Statistical uncertainties are displayed as vertical error bars, while the boxes represent the systematic uncertainties summmed in quadrature. The uncertainties from the luminosity and the branching ratio, that are global to all points are $\pm$ 3.6% which is not drawn on the plots.

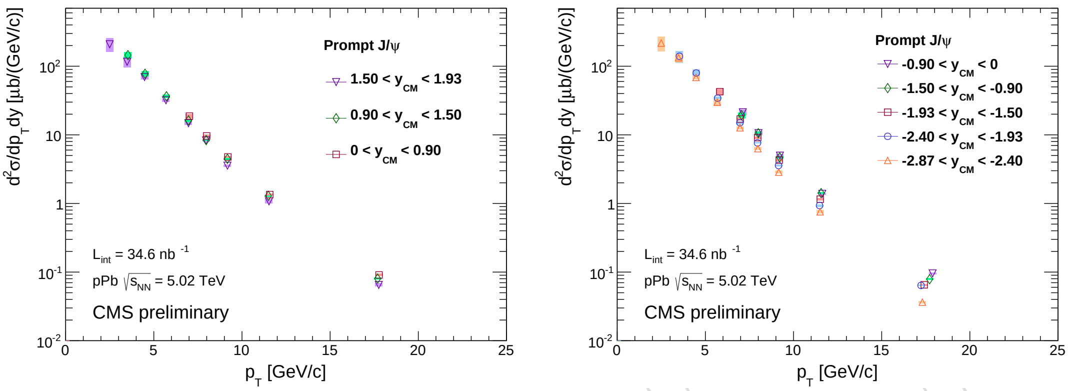

Figure 2: Differential cross section of prompt J/ψ production in the three forward rapidity bins(left) and in the five backward rapidity bins(right). The global uncertainties are $\pm$ 3.6%.

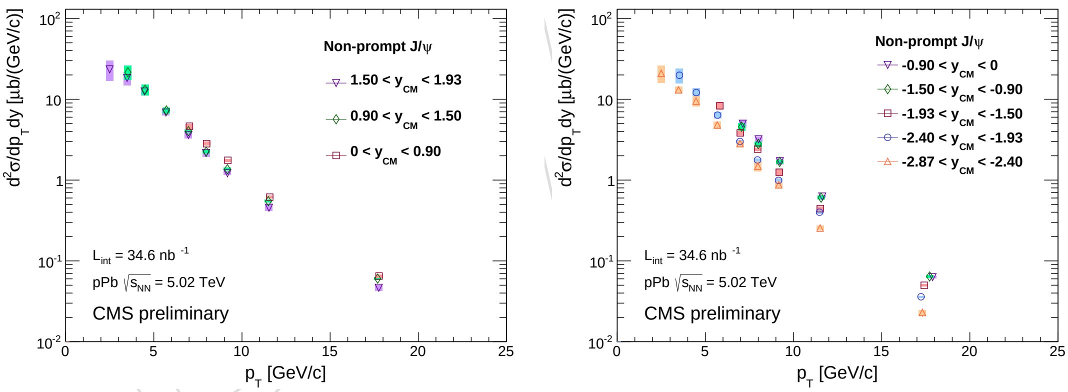

Figure 3: Differential cross section of non-prompt J/ψ production in the three forward rapidity bins(left) and in the five backward rapidity bins(right). The global uncertainties are $\pm$ 3.6%.

In Fig 4, single differential production cross sections are displayed as a function of the center-of-mass rapidity for prompt and non-prompt J/ψ with the integrated p_T regions. Two p_T intervals, $6.5 < p_\mathrm{T} < 10$ GeV/c (Low p_T) and $10 < p_\mathrm{T} < 30$ GeV/c (High p_T) are investigated in order to study the evolution of the shape.

The parton distribution functions in nucleus (nPDFs) is expected to have less values compared to proton PDF, increasingly for lower $x_{1,2}=\frac{m_{\mathrm{J}/\psi}}{\sqrt{s}}e^{\pm y}$. The rapidity dependence of the J/ψ yields provides thus important information on the nPDF modifications. In this paper, the effect was quantified by computing the forward-to-backward production ratio R_{FB} defined by:

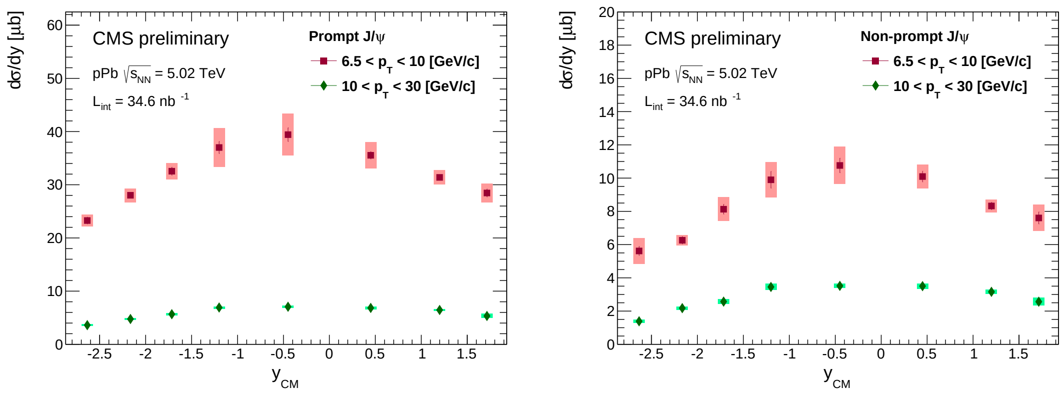

Figure 4: Rapidity dependence of the cross sections for prompt J/ψ (left) and non-prompt J/ψ (right) in the p_T intervals of $6.5 < p_T < 10$ GeV/c (red) and $10 < p_T < 30$ GeV/c (green). The global uncertainties are $\pm$ 3.6%

$$R_{FB} = \frac{N^{fit}_{forward}}{N^{fit}_{backward}} \cdot \frac{A_{backward} \cdot \varepsilon_{backward}}{A_{forward} \cdot \varepsilon_{forward}}, \tag{5}$$

where the variables are defined as

- $N^{fit}_{forward/backward}$ is the raw yield extracted from the fit procedure in the forward or backward rapidity bins,
- $A_{backward/backward}$ is the dimuon acceptance for the forward or backward rapidity bins,
- $\varepsilon_{backward/backward}$ is the dimuon efficiency for the forward or backward rapidity bins.

Fig 5 displays the ratio R_{FB} as a function of p_T in three different rapidity ranges for prompt and non-prompt J/ψ. The data points are plotted at the average of the dimuon p_T inside of each bins. For the rapidity interval $1.5 < |y_{CM}| < 1.93$, the measurement extends down to 5 GeV/c. R_{FB} increases monotonically with p_T, especially for the most forward and backward rapidity bins.

R_{FB} as a function of rapidity for two p_T intervals are shown in Fig 6. No strong rapidity dependence is observed within uncertainties for both prompt and non-prompt J/ψ within the rapidity coverage of the presented measurement, while other experiments in LHC found considerable dependence. It can be understood by the fact that the CMS covers a mid-rapidity region while ALICE[43] and LHCb[44] experiments cover more forward rapidities.

R_{FB} is further analyzed to investigate correlation with the multiplicity-related variable - the transverse energy deposited in the forward hadronic calorimeter in $4 < |\eta| < 5.2$, $E_T^{HF|\eta|>4}$. In table 2, the mean value for each bin is computed from a minimum bias sample. The table also includes the fraction of the minimum bias events in each bin.

Fig 7 shows the ratio R_{FB} as a function of $E_T^{HF|\eta|>4}$ for prompt and non-prompt J/ψ. The centers of the bin abscissae are plotted at their bin-averaged values, but shifted for $6.5 < p_T < 30$ GeV/c points so that they do not overlap with each other. R_{FB} is observed to significantly decrease with $E_T^{HF|\eta|>4}$ in all rapidity bins.

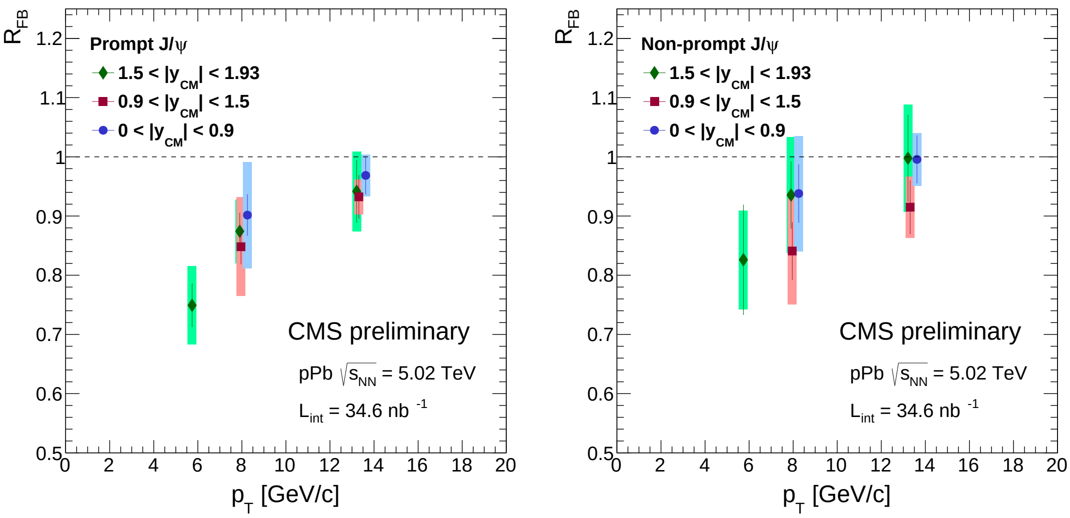

Figure 5: p_{T} dependences of R_{FB} for prompt (left) and non-prompt J/ψ (right) in three rapidity ranges.

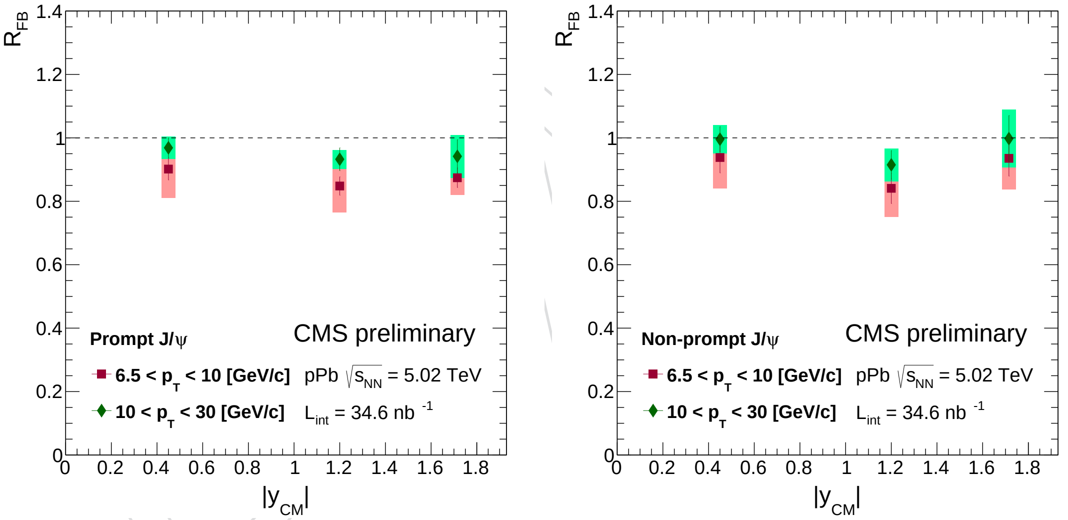

Figure 6: Rapidity distributions of R_{FB} for prompt (left) and non-prompt J/ψ (right) for two selected p_{T} ranges.

Table 2: Definition of the multiplicity-related bins in $E_T^{HF|\eta|>4}$, the mean within the bin, and the fraction of recorded events falling in the bin.

$E_T^{HF|\eta|>4}$ (GeV)	$\langle E_T^{HF|\eta|>4} \rangle$	Fraction in collision events
0–20	9.4	73%
20–30	24.3	18%
30–120	37.2	9%

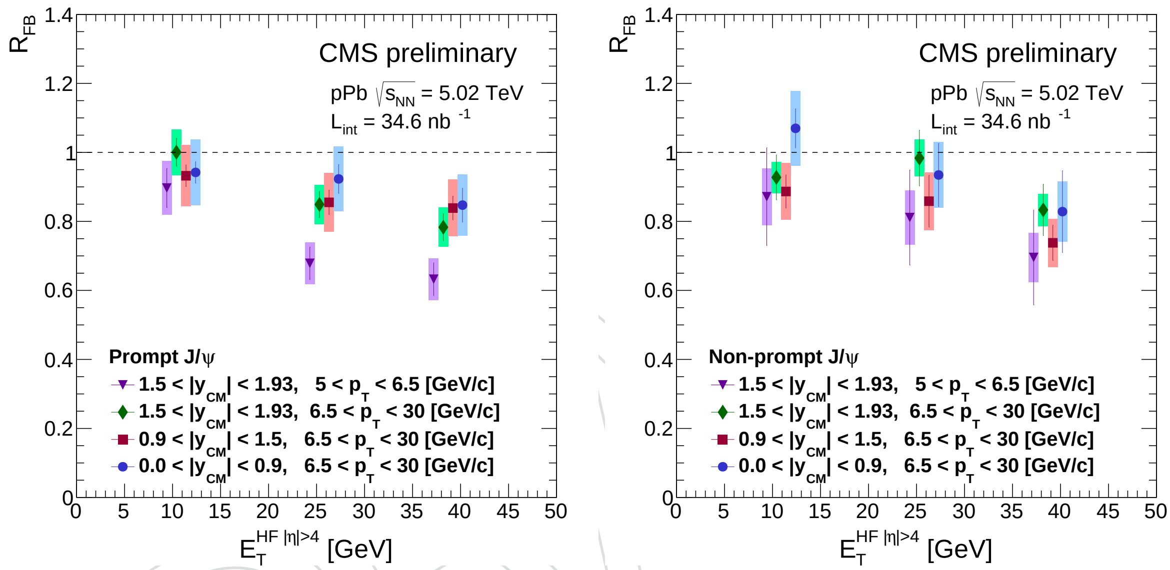

Figure 7: R_{FB} as a function of $E_T^{HF|\eta|>4}$ in three different rapidity ranges for prompt (left) and non-prompt J/ψ (right). The data are integrated over $6.5 < p_T < 30$ GeV/c, and the lower p_T data $5 < p_T < 6.5$ GeV/c is given in addition for the most forward bin $1.5 < |y_{CM}| < 1.93$. For $6.5 < p_T < 30$ GeV/c, the bin abscissae are shifted so that they do not overlap each other.

7.2 Comparision with LHCb and ALICE

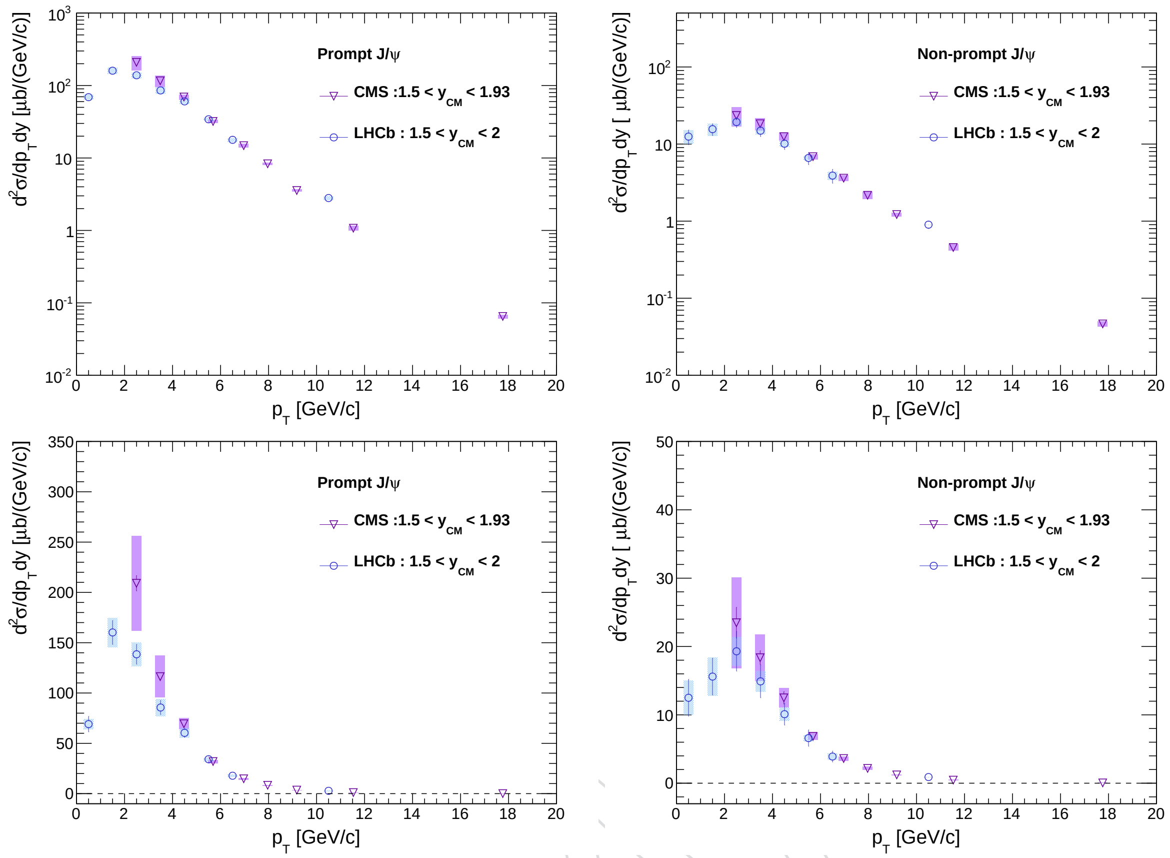

Figure 8: The double differential cross sections as a function of p_T measured by CMS(violet) in pPb collisions and compared to LHCb result(blue) at the same center-of-mass energy. They are represented in log (Top) and linear (Bottom) scale.

The CMS results on R_{FB} are compared with LHCb [44] and ALICE [43] experiments. LHCb collaboration measured the prompt and non-promt J/ψ in rapidity range of $1.5 < y_C M < 4.0$ and transverse momentum range of $0 < p_T < 14$ GeV/c. ALICE measured the inclusive J/ψ in range of $2.96 < y_C M < 3.53$ and $0 < p_T < 15$ GeV/c. For the similarity in kinematic range, the CMS spectra result at the most forward region $1.5 < y_{CM} < 1.93$ was compared to LHCb result in the range of $1.5 < y_C M < 2.0$ as shown in Fig. 8. The top and bottom panel are same plots depicted in log and linear scale respectively. The CMS data points are equivalent to those in Fig. 2 and Fig. 3.

In addition, the R_{FB} as a function of p_T measured by CMS, LHCb and ALICE are compared in Figure 9. Note that the CMS measuerment covers more central rapidity range $1.5 < |y_{CM}| < 1.93$, whereas LHCb and ALICE coveres $2.5 < |y_{CM}| < 4$ and $2.96 < y_C M < 3.53$ respectively. The ALICE data points are inclusive J/ψ wihtout separating non-prompt. The similar p_T dependence tendency is found for all 3 experiments in spite of inconsistent rapidity intervals. Finally, the rapidity dependence of the R_{FB} is compared to LHCb and ALICE in figure 10 by integrating double differential cross seciontion by p_T. The R_{FB} is observed to be close to the unity for mid-rapidity (CMS) and it gradually decreases at forward rapidity (ALICE and LHCb), which implies the significant modification of nPDF at low x region in lead nucleus.

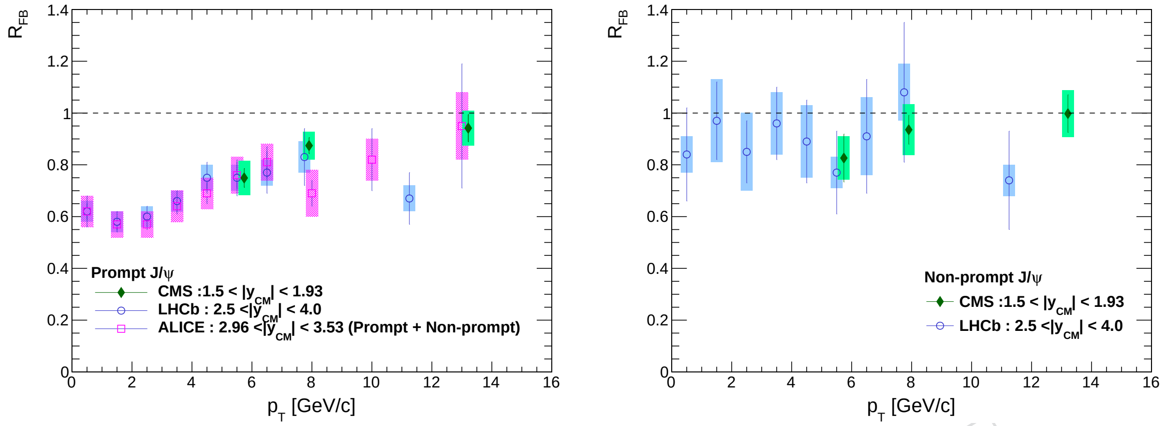

Figure 9: Transverse momentum dependence of R_{FB} measured by CMS(green), LHCb(blue) and ALICE(magenta) at the same center-of-mass energy pPb collision.

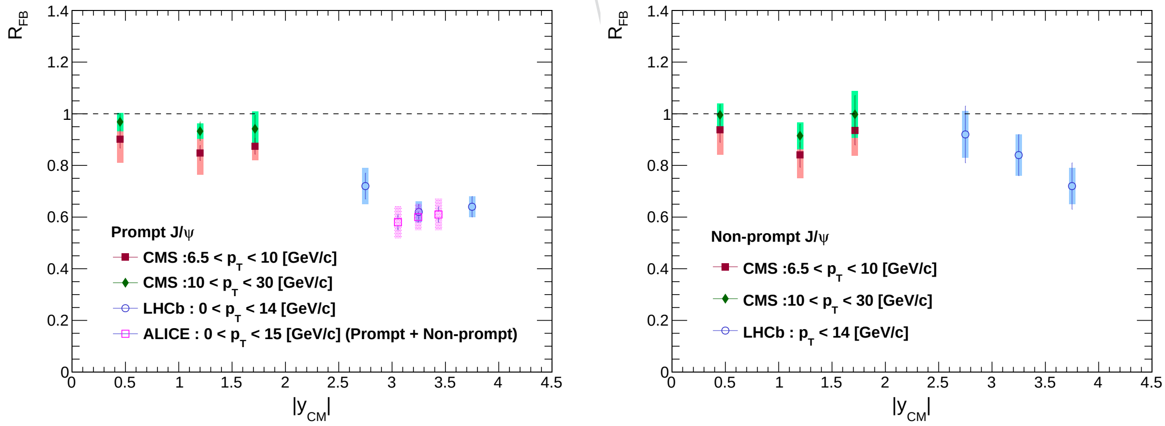

Figure 10: Rapidity dependence of R_{FB} measured by CMS(green and red for high p_T and low p_T respectively), LHCb(blue) and ALICE(magenta).

Table 3: double differential cross section of prompt J/ψ as functions of rapidity, and p_T. Quoted uncertainties are statistical and systematic.

y_{CM}(J/ψ)	p_T(J/ψ) [GeV/c]	$\langle p_T(J/\psi)\rangle$	$\frac{d^2\sigma}{dp_T dy}$ [μb/(GeV/c)]
	$2.0 \leq p_T < 3.0$	2.50	209.11± 7.63 ±47.06
	$3.0 \leq p_T < 4.0$	3.49	116.33± 3.08 ±20.67
	$4.0 \leq p_T < 5.0$	4.47	69.49± 2.24 ±5.66
	$5.0 \leq p_T < 6.5$	5.69	31.93± 0.93 ±1.53
$1.5 \leq y < 1.93$	$6.5 \leq p_T < 7.5$	6.96	14.79± 0.57 ±0.91
	$7.5 \leq p_T < 8.5$	7.96	8.32± 0.40 ±0.30
	$8.5 \leq p_T < 10.0$	9,18	3.56± 0.19 ±0.12
	$10.0 \leq p_T < 14.0$	11.53	1.07± 0.06 ±0.08
	$14.0 \leq p_T < 30.0$	17.76	0.065±0.005±0.004
	$3.0 \leq p_T < 4.0$	3.51	144.99± 4.65 ±15.04
	$4.0 \leq p_T < 5.0$	4.50	77.76± 2.16 ±7.00
	$5.0 \leq p_T < 6.5$	5.72	36.47± 0.75 ±1.92
$0.9 \leq y < 1.5$	$6.5 \leq p_T < 7.5$	6.97	16.28± 0.37 ±0.70
	$7.5 \leq p_T < 8.5$	7.97	8.38± 0.22 ±0.23
	$8.5 \leq p_T < 10.0$	9.17	4.48± 0.12 ±0.12
	$10.0 \leq p_T < 14.0$	11.50	1.30± 0.04 ±0.04
	$14.0 \leq p_T < 30.0$	17.69	0.080±0.004±0.002
	$6.5 \leq p_T < 7.5$	7.02	18.76± 0.61 ±1.30
	$7.5 \leq p_T < 8.5$	8.00	9.64± 0.30 ±0.45
$0.0 \leq y < 0.9$	$8.5 \leq p_T < 10.0$	9.20	4.76± 0.13 ±0.15
	$10.0 \leq p_T < 14.0$	11.57	1.35± 0.04 ±0.04
	$14.0 \leq p_T < 30.0$	17.77	0.091±0.003±0.003
	$6.5 \leq p_T < 7.5$	7.12	21.36± 1.19 ±2.13
	$7.5 \leq p_T < 8.5$	8.01	10.59± 0.42 ±0.66
$-0.9 \leq y < 0.0$	$8.5 \leq p_T < 10.0$	9.23	4.98± 0.18 ±0.21
	$10.0 \leq p_T < 14.0$	11.63	1.38± 0.04 ±0.03
	$14.0 \leq p_T < 30.0$	17.89	0.096±0.004±0.003
	$6.5 \leq p_T < 7.5$	7.05	19.40± 1.02 ±1.91
	$7.5 \leq p_T < 8.5$	8.00	10.55± 0.44 ±0.63
$-1.5 \leq y < -0.9$	$8.5 \leq p_T < 10.0$	9.22	4.71± 0.18 ±0.17
	$10.0 \leq p_T < 14.0$	11.56	1.42± 0.05 ±0.04
	$14.0 \leq p_T < 30.0$	17.72	0.079±0.004±0.002
	$5.0 \leq p_T < 6.5$	5.82	42.62± 1.65 ±3.75
	$6.5 \leq p_T < 7.5$	6.98	17.00± 0.62 ±0.80
$-1.93 \leq y < -1.5$	$7.5 \leq p_T < 8.5$	7.97	9.12± 0.37 ±0.31
	$8.5 \leq p_T < 10.0$	9.19	4.29± 0.17 ±0.15
	$10.0 \leq p_T < 14.0$	11.52	1.15± 0.04 ±0.04
	$14.0 \leq p_T < 30.0$	17.41	0.065±0.004±0.002
	$3.0 \leq p_T < 4.0$	3.53	139.64± 4.86 ±27.41
	$4.0 \leq p_T < 5.0$	4.48	79.769± 2.18 ±9.68
	$5.0 \leq p_T < 6.5$	5.69	34.23± 0.74 ±1.69
$-2.4 \leq y < -1.93$	$6.5 \leq p_T < 7.5$	6.96	15.02± 0.42 ±0.70
	$7.5 \leq p_T < 8.5$	7.96	7.64± 0.26 ±0.19
	$8.5 \leq p_T < 10.0$	9.15	3.58± 0.12 ±0.09
	$10.0 \leq p_T < 14.0$	11.47	0.93± 0.04 ±0.03
	$14.0 \leq p_T < 30.0$	17.23	0.064±0.004±0.002
	$2.0 \leq p_T < 3.0$	2.49	217.53± 7.05 ±52.61
	$3.0 \leq p_T < 4.0$	3.48	132.87± 3.78 ±18.26
	$4.0 \leq p_T < 5.0$	4.47	68.66± 1.96 ±4.10
	$5.0 \leq p_T < 6.5$	5.68	29.94± 0.86 ±3.35
$-2.87 \leq y < -2.4$	$6.5 \leq p_T < 7.5$	6.96	12.70± 0.52 ±0.61
	$7.5 \leq p_T < 8.5$	7.98	6.29± 0.30 ±0.28
	$8.5 \leq p_T < 10.0$	9.16	2.86± 0.15 ±0.13
	$10.0 \leq p_T < 14.0$	11.51	0.76± 0.04 ±0.04
	$14.0 \leq p_T < 30.0$	17.31	0.036±0.004±0.001

Table 4: double differential cross section of non-prompt J/ψ as functions of rapidity, and p_{T}. Quoted uncertainties are statistical and systematic.

y_{CM}(J/ψ)	p_{T}(J/ψ) [GeV/c]	$\langle p_{\mathrm{T}}(\mathrm{J}/\psi)\rangle$ [GeV/c]	$\frac{d^2\sigma}{dp_{\mathrm{T}}dy}$[$\mu b$/(GeV/$c$)]
$1.5 \le y < 1.93$	$2.0 \le p_{\mathrm{T}} < 3.0$	2.50	23.48± 2.26 ±6.65
	$3.0 \le p_{\mathrm{T}} < 4.0$	3.49	18.37± 1.02 ±3.39
	$4.0 \le p_{\mathrm{T}} < 5.0$	4.47	12.49± 0.93 ±1.40
	$5.0 \le p_{\mathrm{T}} < 6.5$	5.69	6.86± 0.41 ±0.54
	$6.5 \le p_{\mathrm{T}} < 7.5$	6.96	3.61± 0.25 ±0.32
	$7.5 \le p_{\mathrm{T}} < 8.5$	7.96	2.17± 0.19 ±0.23
	$8.5 \le p_{\mathrm{T}} < 10.0$	9,18	1.22± 0.12 ±0.07
	$10.0 \le p_{\mathrm{T}} < 14.0$	11.53	0.46± 0.03 ±0.04
	$14.0 \le p_{\mathrm{T}} < 30.0$	17.76	0.046±0.004±0.004
$0.9 \le y < 1.5$	$3.0 \le p_{\mathrm{T}} < 4.0$	3.51	21.60± 1.77 ±4.31
	$4.0 \le p_{\mathrm{T}} < 5.0$	4.50	13.12± 0.68 ±1.97
	$5.0 \le p_{\mathrm{T}} < 6.5$	5.72	7.27± 0.40 ±0.58
	$6.5 \le p_{\mathrm{T}} < 7.5$	6.97	4.03± 0.17 ±0.15
	$7.5 \le p_{\mathrm{T}} < 8.5$	7.97	2.25± 0.11 ±0.11
	$8.5 \le p_{\mathrm{T}} < 10.0$	9.17	1.36± 0.05 ±0.06
	$10.0 \le p_{\mathrm{T}} < 14.0$	11.50	0.55± 0.03 ±0.02
	$14.0 \le p_{\mathrm{T}} < 30.0$	17.69	0.060±0.003±0.002
$0.0 \le y < 0.9$	$6.5 \le p_{\mathrm{T}} < 7.5$	7.02	4.64± 0.27 ±0.33
	$7.5 \le p_{\mathrm{T}} < 8.5$	8.00	2.82± 0.15 ±0.15
	$8.5 \le p_{\mathrm{T}} < 10.0$	9.20	1.76± 0.08 ±0.08
	$10.0 \le p_{\mathrm{T}} < 14.0$	11.57	0.62± 0.02 ±0.03
	$14.0 \le p_{\mathrm{T}} < 30.0$	17.77	0.065±0.002±0.003
$-0.9 \le y < 0.0$	$6.5 \le p_{\mathrm{T}} < 7.5$	7.12	4.99± 0.37 ±0.52
	$7.5 \le p_{\mathrm{T}} < 8.5$	8.01	3.20± 0.18 ±0.23
	$8.5 \le p_{\mathrm{T}} < 10.0$	9.23	1.72± 0.11 ±0.13
	$10.0 \le p_{\mathrm{T}} < 14.0$	11.63	0.63± 0.02 ±0.02
	$14.0 \le p_{\mathrm{T}} < 30.0$	17.89	0.063±0.003±0.002
$-1.5 \le y < -0.9$	$6.5 \le p_{\mathrm{T}} < 7.5$	7.05	4.58± 0.44 ±0.49
	$7.5 \le p_{\mathrm{T}} < 8.5$	8.00	2.80± 0.20 ±0.21
	$8.5 \le p_{\mathrm{T}} < 10.0$	9.22	1.68± 0.10 ±0.09
	$10.0 \le p_{\mathrm{T}} < 14.0$	11.56	0.61± 0.03 ±0.03
	$14.0 \le p_{\mathrm{T}} < 30.0$	17.72	0.064±0.004±0.002
$-1.93 \le y < -1.5$	$5.0 \le p_{\mathrm{T}} < 6.5$	5.82	8.30± 0.78 ±0.84
	$6.5 \le p_{\mathrm{T}} < 7.5$	6.98	3.84± 0.19 ±0.26
	$7.5 \le p_{\mathrm{T}} < 8.5$	7.97	2.41± 0.19 ±0.11
	$8.5 \le p_{\mathrm{T}} < 10.0$	9.19	1.25± 0.08 ±0.11
	$10.0 \le p_{\mathrm{T}} < 14.0$	11.52	0.44± 0.03 ±0.02
	$14.0 \le p_{\mathrm{T}} < 30.0$	17.41	0.050±0.003±0.002
$-2.4 \le y < -1.93$	$3.0 \le p_{\mathrm{T}} < 4.0$	3.53	19.83± 1.85 ±4.08
	$4.0 \le p_{\mathrm{T}} < 5.0$	4.48	12.11± 0.62 ±1.63
	$5.0 \le p_{\mathrm{T}} < 6.5$	5.69	6.36± 0.34 ±0.56
	$6.5 \le p_{\mathrm{T}} < 7.5$	6.96	3.00± 0.15 ±0.13
	$7.5 \le p_{\mathrm{T}} < 8.5$	7.96	1.78± 0.12 ±0.07
	$8.5 \le p_{\mathrm{T}} < 10.0$	9.15	0.99± 0.06 ±0.05
	$10.0 \le p_{\mathrm{T}} < 14.0$	11.47	0.40± 0.03 ±0.02
	$14.0 \le p_{\mathrm{T}} < 30.0$	17.23	0.036±0.003±0.001
$-2.87 \le y < -2.4$	$2.0 \le p_{\mathrm{T}} < 3.0$	2.49	20.90± 2.05 ±5.04
	$3.0 \le p_{\mathrm{T}} < 4.0$	3.48	13.08± 1.15 ±1.22
	$4.0 \le p_{\mathrm{T}} < 5.0$	4.47	9.49± 0.71 ±1.38
	$5.0 \le p_{\mathrm{T}} < 6.5$	5.68	4.81± 0.37 ±0.48
	$6.5 \le p_{\mathrm{T}} < 7.5$	6.96	2.82± 0.22 ±0.21
	$7.5 \le p_{\mathrm{T}} < 8.5$	7.98	1.48± 0.10 ±0.20
	$8.5 \le p_{\mathrm{T}} < 10.0$	9.16	0.87± 0.08 ±0.08
	$10.0 \le p_{\mathrm{T}} < 14.0$	11.51	0.25± 0.02 ±0.02
	$14.0 \le p_{\mathrm{T}} < 30.0$	17.31	0.023±0.003±0.002

Table 5: R_{FB} of prompt J/ψ as functions of rapidity, and p_{T}. Quoted uncertainties are statistical and systematic.

$\lvert y_{CM}(\mathrm{J}/\psi)\rvert$	$p_{\mathrm{T}}(\mathrm{J}/\psi)$ [GeV/c]	$\langle p_{\mathrm{T}}(\mathrm{J}/\psi)\rangle$	R_{FB}
$1.5 \leq \lvert y\rvert < 1.93$	$5.0 \leq p_{\mathrm{T}} < 6.5$	5.74	0.75±0.04±0.07
	$6.5 \leq p_{\mathrm{T}} < 10.0$	7.90	0.87±0.03±0.05
	$10.0 \leq p_{\mathrm{T}} < 30.0$	13.21	0.94±0.05±0.07
$0.9 \leq \lvert y\rvert < 1.5$	$6.5 \leq p_{\mathrm{T}} < 10.0$	7.96	0.85±0.03±0.08
	$10.0 \leq p_{\mathrm{T}} < 30.0$	13.31	0.93±0.04±0.03
$0.0 \leq \lvert y\rvert < 0.9$	$6.5 \leq p_{\mathrm{T}} < 10.0$	8.25	0.90±0.03±0.09
	$10.0 \leq p_{\mathrm{T}} < 30.0$	13.62	0.97±0.03±0.04

Table 6: R_{FB} of non-prompt J/ψ as function of rapidity, and p_{T}. Quoted uncertainties are statistical and systematic.

$\lvert y_{CM}(\mathrm{J}/\psi)\rvert$	$p_{\mathrm{T}}(\mathrm{J}/\psi)$ [GeV/c]	$\langle p_{\mathrm{T}}(\mathrm{J}/\psi)\rangle$	R_{FB}
$1.5 \leq \lvert y\rvert < 1.93$	$5.0 \leq p_{\mathrm{T}} < 6.5$	5.74	0.83±0.09±0.08
	$6.5 \leq p_{\mathrm{T}} < 10.0$	7.90	0.94±0.06±0.10
	$10.0 \leq p_{\mathrm{T}} < 30.0$	13.21	1.00±0.07±0.09
$0.9 \leq \lvert y\rvert < 1.5$	$6.5 \leq p_{\mathrm{T}} < 10.0$	7.96	0.84±0.05±0.09
	$10.0 \leq p_{\mathrm{T}} < 30.0$	13.31	0.91±0.05±0.05
$0.0 \leq \lvert y\rvert < 0.9$	$6.5 \leq p_{\mathrm{T}} < 10.0$	8.25	0.93±0.05±0.10
	$10.0 \leq p_{\mathrm{T}} < 30.0$	13.62	1.00±0.04±0.04

Table 7: R_{FB} of prompt J/ψ as functions of rapidity, p_{T}, and $E_T^{HF|\eta|>4}$. Quoted uncertainties are statistical and systematic.

$\lvert y_C M(\mathrm{J}/\psi)\rvert$	$p_{\mathrm{T}}(\mathrm{J}/\psi)$ [GeV/c]	$E_T^{HF\lvert\eta\rvert>4}$ [GeV/c]	R_{FB}
$1.5 \leq \lvert y\rvert < 1.93$	$5.0 \leq p_{\mathrm{T}} < 6.5$	0–20	0.90±0.06±0.08
	$6.5 \leq p_{\mathrm{T}} < 30.0$		1.00±0.04±0.07
$1.5 \leq \lvert y\rvert < 1.93$	$5.0 \leq p_{\mathrm{T}} < 6.5$	20–30	0.68±0.05±0.06
	$6.5 \leq p_{\mathrm{T}} < 30.0$		0.85±0.04±0.06
$1.5 \leq \lvert y\rvert < 1.93$	$5.0 \leq p_{\mathrm{T}} < 6.5$	30–120	0.63±0.05±0.06
	$6.5 \leq p_{\mathrm{T}} < 30.0$		0.78±0.04±0.06
$0.9 \leq \lvert y\rvert < 1.5$	$6.5 \leq p_{\mathrm{T}} < 30.0$	0–20	0.93±0.03±0.09
$0.9 \leq \lvert y\rvert < 1.5$	$6.5 \leq p_{\mathrm{T}} < 30.0$	20–30	0.86±0.04±0.09
$0.9 \leq \lvert y\rvert < 1.5$	$6.5 \leq p_{\mathrm{T}} < 30.0$	30–120	0.84±0.03±0.09
$0.0 \leq \lvert y\rvert < 0.9$	$6.5 \leq p_{\mathrm{T}} < 30.0$	0–20	0.94±0.03±0.09
$0.0 \leq \lvert y\rvert < 0.9$	$6.5 \leq p_{\mathrm{T}} < 30.0$	20–30	0.92±0.04±0.09
$0.0 \leq \lvert y\rvert < 0.9$	$6.5 \leq p_{\mathrm{T}} < 30.0$	30–120	0.85±0.05±0.09

Table 8: R_{FB} of non-prompt J/ψ as functions of rapidity, p_{T}, and $E_T^{HF|\eta|>4}$. Quoted uncertainties are statistical and systematic.

$\lvert y_C M(\mathrm{J}/\psi)\rvert$	$p_{\mathrm{T}}(\mathrm{J}/\psi)$ [GeV/c]	$E_T^{HF\lvert\eta\rvert>4}$ [GeV/c]	R_{FB}
$1.5 \leq \lvert y\rvert < 1.93$	$5.0 \leq p_{\mathrm{T}} < 6.5$	0–20	0.87±0.14±0.08
	$6.5 \leq p_{\mathrm{T}} < 30.0$		0.93±0.07±0.05
$1.5 \leq \lvert y\rvert < 1.93$	$5.0 \leq p_{\mathrm{T}} < 6.5$	20–30	0.81±0.14±0.08
	$6.5 \leq p_{\mathrm{T}} < 30.0$		0.98±0.08±0.05
$1.5 \leq \lvert y\rvert < 1.93$	$5.0 \leq p_{\mathrm{T}} < 6.5$	30–120	0.70±0.14±0.07
	$6.5 \leq p_{\mathrm{T}} < 30.0$		0.83±0.07±0.05
$0.9 \leq \lvert y\rvert < 1.5$	$6.5 \leq p_{\mathrm{T}} < 30.0$	0–20	0.89±0.05±0.08
$0.9 \leq \lvert y\rvert < 1.5$	$6.5 \leq p_{\mathrm{T}} < 30.0$	20–30	0.86±0.08±0.08
$0.9 \leq \lvert y\rvert < 1.5$	$6.5 \leq p_{\mathrm{T}} < 30.0$	30–120	0.74±0.05±0.07
$0.0 \leq \lvert y\rvert < 0.9$	$6.5 \leq p_{\mathrm{T}} < 30.0$	0–20	1.07±0.06±0.11
$0.0 \leq \lvert y\rvert < 0.9$	$6.5 \leq p_{\mathrm{T}} < 30.0$	20–30	0.93±0.09±0.10
$0.0 \leq \lvert y\rvert < 0.9$	$6.5 \leq p_{\mathrm{T}} < 30.0$	30–120	0.83±0.12±0.09

8 Summary

The CMS detector at LHC has been used to investigate prompt and non-prompt J/ψ production in pPb collisions at $\sqrt{s_{\rm NN}} = 5.02$ TeV. The data sample corresponds to an integrated luminosity of 34.6 nb^{-1}. This paper reports the ($p_{\rm T}$, y) differential production rates of J/ψ measured in the rapidity range of $-2.4 < y_{CM} < 1.93$. In addition, the ratio of forward-backward yields, R_{FB} as a function of $p_{\rm T}$ and rapidity, has been measured. The R_{FB} is found to be $\sim$0.7 at low $p_{\rm T}$ but increases to become consistent with unity at $p_{\rm T} > \sim 10$ GeV/c. The correlation between the R_{FB} and the multiplicity-related variable, $E_T^{HF|\eta|>4}$ has been also studied. In the largest $E_T^{HF|\eta|>4}$ bin, the R_{FB} in the rapidity range of $1.5 < |y_{CM}| < 1.93$ and $5 < p_{\rm T}6.5$ GeV/c are 0.55 ± 0.04(stat.) $\pm$ 0.02(sys.) and 0.66$\pm$0.11(stat.)$\pm$0.10(sys.) for prompt and non-prompt J/ψ, respectively.

References

[1] S. Gavin and R. Vogt, “J/ψ Suppression From Hadron - Nucleus to Nucleus-nucleus Collisions”, *Nucl.Phys.* **B345** (1990) 104–124, doi:10.1016/0550-3213(90)90610-P.

[2] T. Matsui and H. Satz, “J/ψ suppression by quark-gluon plasma formation”, *Phys. Lett. B* **178** (1986) 416, doi:10.1016/0370-2693(86)91404-8.

[3] R. Vogt, “Cold Nuclear Matter Effects on J/ψ and Υ Production at energies available at the CERN Large Hadron Collider (LHC)”, *Phys. Rev. C* **81** (2010) 044903, doi:10.1103/PhysRevC.81.044903, arXiv:1003.3497.

[4] C. Lourenco, R. Vogt, and H. K. Woehri, “Energy dependence of J/ψ absorption in proton-nucleus collisions”, *JHEP* **02** (2009) 014, doi:10.1088/1126-6708/2009/02/014, arXiv:0901.3054.

[5] LHCb Collaboration, “Measurement of the fraction of $\Upsilon(1S)$ originating from $\chi_b(1P)$ decays in pp collisions at $\sqrt{s} = 7$ TeV”, *JHEP* **1211** (2012) 031, doi:10.1007/JHEP11(2012)031, arXiv:1209.0282.

[6] NA38 Collaboration, “ψ' and J/ψ production in pW, pU and SU interactions at 200 GeV/nucleon”, *Phys. Lett. B* **345** (1995) 617, doi:10.1016/0370-2693(94)01614-I.

[7] CMS Collaboration, “Suppression of non-prompt J/ψ, prompt J/ψ, and Υ(1S) in PbPb collisions at $\sqrt{s_{\rm NN}} = 2.76$ TeV”, *JHEP* **05** (2012) 063, doi:10.1007/JHEP05(2012)063, arXiv:1201.5069.

[8] ALICE Collaboration, “J/ψ Production as a Function of Charged Particle Multiplicity in pp Collisions at $\sqrt{s} = 7$ TeV”, *Phys.Lett.* **B712** (2012) 165–175, doi:10.1016/j.physletb.2012.04.052, arXiv:1202.2816.

[9] Quarkonium Working Group Collaboration, “Heavy quarkonium physics”, arXiv:hep-ph/0412158.

[10] J. Lansberg, “J/ψ, ψ ' and υ production at hadron colliders: A Review”, *Int.J.Mod.Phys.* **A21** (2006) 3857–3916, doi:10.1142/S0217751X06033180, arXiv:hep-ph/0602091.

[11] M. Kramer, “Quarkonium production at high-energy colliders”, *Progress in Particle and Nuclear Physics* **47** (2001), no. 1, 141 – 201, doi:http://dx.doi.org/10.1016/S0146-6410(01)00154-5.

[12] N. Brambilla et al., "Heavy quarkonium: progress, puzzles, and opportunities", *Eur.Phys.J.* **C71** (2011) 1534, doi:10.1140/epjc/s10052-010-1534-9, arXiv:1010.5827.

[13] P. Artoisenet, J. Lansberg, and F. Maltoni, "Hadroproduction of and in association with a heavy-quark pair", *Physics Letters B* **653** (2007), no. 1, 60 – 66, doi:http://dx.doi.org/10.1016/j.physletb.2007.04.031.

[14] CMS Collaboration, "J/ψ and ψ_{2S} production in pp collisions at $\sqrt{s} = 7$ TeV", *JHEP* **1202** (2012) 011, doi:10.1007/JHEP02(2012)011, arXiv:1111.1557.

[15] ALICE Collaboration, "Rapidity and transverse momentum dependence of inclusive J/psi production in pp collisions at $\sqrt{s} = 7$ TeV", *Phys.Lett.* **B704** (2011) 442–455, doi:10.1016/j.physletb.2011.09.054,10.1016/j.physletb.2012.10.060, arXiv:1105.0380.

[16] LHCb Collaboration, "Measurement of J/ψ production in pp collisions at $\sqrt{s} = 7$ TeV", *Eur.Phys.J.* **C71** (2011) 1645, doi:10.1140/epjc/s10052-011-1645-y, arXiv:1103.0423.

[17] ATLAS Collaboration Collaboration, "Measurement of the differential cross-sections of inclusive, prompt and non-prompt J/ψ production in proton-proton collisions at $\sqrt{s} = 7$ TeV", *Nucl.Phys.* **B850** (2011) 387–444, doi:10.1016/j.nuclphysb.2011.05.015, arXiv:1104.3038.

[18] Y.-Q. Ma, K. Wang, and K.-T. Chao, "$J/\psi(\psi')$ production at the Tevatron and LHC at $\mathcal{O}(\alpha_s^4 v^4)$ in nonrelativistic QCD", *Phys.Rev.Lett.* **106** (2011) 042002, doi:10.1103/PhysRevLett.106.042002, arXiv:1009.3655.

[19] NA50 Collaboration, "Anomalous J/ψ suppression in Pb + Pb collisions at 158-A-GeV/c", *Nucl.Phys.* **A610** (1996) 404C–417C, doi:10.1016/S0375-9474(96)00373-9.

[20] NA50 Collaboration, "Anomalous J/ψ suppression in Pb + Pb interactions at 158 GeV/c per nucleon", *Phys.Lett.* **B410** (1997) 337–343, doi:10.1016/S0370-2693(97)00915-5.

[21] PHENIX Collaboration, "J/ψ Production vs Centrality, Transverse Momentum, and Rapidity in Au+Au Collisions at $\sqrt{s_{NN}} = 200$ GeV", *Phys.Rev.Lett.* **98** (2007) 232301, doi:10.1103/PhysRevLett.98.232301, arXiv:nucl-ex/0611020.

[22] PHENIX Collaboration, "J/ψ Production in s(NN)**(1/2) = 200-GeV Cu+Cu Collisions", *Phys.Rev.Lett.* **101** (2008) 122301, doi:10.1103/PhysRevLett.101.122301, arXiv:0801.0220.

[23] aboration Collaboration, "Centrality, rapidity and transverse momentum dependence of J/ψ suppression in Pb-Pb collisions at $\sqrt{s_{NN}}$=2.76TeV", arXiv:1311.0214.

[24] S. Digal, P. Petreczky, and H. Satz, "Quarkonium feed down and sequential suppression", *Phys.Rev.* **D64** (2001) 094015, doi:10.1103/PhysRevD.64.094015, arXiv:hep-ph/0106017.

[25] Á. Mócsy and P. Petreczky, "Color screening melts quarkonium", *Phys. Rev. Lett.* **99** (2007) 211602, doi:10.1103/PhysRevLett.99.211602, arXiv:0706.2183.

[26] A. Mocsy, “Potential Models for Quarkonia”, *Eur. Phys. J. C* **61** (2009) 705, doi:10.1140/epjc/s10052-008-0847-4, arXiv:0811.0337.

[27] C. J. Benesh, J.-w. Qiu, and J. P. Vary, “J / psi suppression in hadron - nucleus collisions”, *Phys.Rev.* **C50** (1994) 1015–1023, doi:10.1103/PhysRevC.50.1015, arXiv:hep-ph/9403265.

[28] H. Fujii, F. Gelis, and R. Venugopalan, “Quark pair production in high energy pA collisions: General features”, *Nucl.Phys.* **A780** (2006) 146–174, doi:10.1016/j.nuclphysa.2006.09.012, arXiv:hep-ph/0603099.

[29] R. Sharma and I. Vitev, “High transverse momentum quarkonium production and dissociation in heavy ion collisions”, *Phys.Rev.* **C87** (2013), no. 4, 044905, doi:10.1103/PhysRevC.87.044905, arXiv:1203.0329.

[30] F. Arleo and S. Peigne, “Heavy-quarkonium suppression in p-A collisions from parton energy loss in cold QCD matter”, *JHEP* **1303** (2013) 122, doi:10.1007/JHEP03(2013)122, arXiv:1212.0434.

[31] F. Arleo, R. Kolevatov, S. Peign, and M. Rustamova, “Centrality and $p_\perp$ dependence of J/ψ suppression in proton-nucleus collisions from parton energy loss”, *JHEP* **1305** (2013) 155, doi:10.1007/JHEP05(2013)155, arXiv:1304.0901.

[32] R. Vogt, “Shadowing and absorption effects on J/psi production in dA collisions”, *Phys.Rev.* **C71** (2005) 054902, doi:10.1103/PhysRevC.71.054902, arXiv:hep-ph/0411378.

[33] CMS Collaboration, “The CMS experiment at the CERN LHC”, *JINST* **3** (2008) S08004, doi:10.1088/1748-0221/3/08/S08004.

[34] CMS Collaboration, “Multiplicity and transverse-momentum dependence of two- and four-particle correlations in pPb and PbPb collisions”, arXiv:1305.0609.

[35] J. Gaiser, “Charmonium Spectroscopy From Radiative Decays of the J/ψ and ψ'”,.

[36] ALEPH Collaboration, “Measurement of the $\overline{\mathrm{B}}^0$ and B^- meson lifetimes”, *Phys. Lett. B* **307** (1993) 194, doi:10.1016/0370-2693(93)90211-Y.

[37] ALEPH Collaboration, “Errata: Measurement of the $\overline{\mathrm{B}}^0$ and B^- meson lifetimes”, *Phys. Lett. B* **325** (1994) 537, doi:10.1016/0370-2693(94)90054-X.

[38] T. Sjostrand, S. Mrenna, and P. Z. Skands, “PYTHIA 6.4 Physics and Manual”, *JHEP* **0605** (2006) 026, doi:10.1088/1126-6708/2006/05/026, arXiv:hep-ph/0603175.

[39] D. J. Lange, “The EvtGen particle decay simulation package”, *Nucl. Instrum. Meth. A* **462** (2001) 152, doi:10.1016/S0168-9002(01)00089-4.

[40] E. Barberio, B. van Eijk, and Z. Was, “PHOTOS: A universal Monte Carlo for QED radiative corrections in decays”, *Comput. Phys. Commun.* **66** (1991) 115, doi:10.1016/0010-4655(91)90012-A.

[41] GEANT Collaboration, “GEANT4 — A simulation toolkit”, *Nucl. Instrum. Meth. A* **506** (2003) 250, doi:10.1016/S0168-9002(03)01368-8.

[42] Particle Data Group Collaboration, "Review of Particle Physics (RPP)", *Phys.Rev.* **D86** (2012) 010001, doi:10.1103/PhysRevD.86.010001.

[43] ALICE Collaboration, "J/ψ production and nuclear effects in p-Pb collisions at $\sqrt{S_{NN}}$ = 5.02 TeV", *JHEP* **1402** (2014) 073, doi:10.1007/JHEP02(2014)073, arXiv:1308.6726.

[44] LHCb Collaboration, "Study of J/ψ production and cold nuclear matter effects in pPb collisions at $\sqrt{s_{NN}} = 5$ TeV", *JHEP* **1402** (2014) 072, doi:10.1007/JHEP02(2014)072, arXiv:1308.6729.